X-valley leakage in GaAs/AlGaAs quantum cascade lasers

X. Gao, D. Botez, and I. Knezevic[a)]
Department of Electrical and Computer Engineering, University of Wisconsin-Madison, 1415 Engineering Dr., Madison, Wisconsin 53706-1691

(Received 12 June 2006; accepted 25 September 2006; published online 9 November 2006)

The authors present a Monte Carlo simulation of GaAs/$Al_{0.33}Ga_{0.67}As$ and GaAs/$Al_{0.45}Ga_{0.55}As$ quantum cascade lasers (QCLs) that incorporates both Γ- and *X*-valley transport. The dominant *X*-valley leakage path in both lasers is interstage $X \to X$ scattering. The leakage current is much higher in the 33%-Al QCL, as strong coupling of its weakly localized Γ-valley states to the next-stage continuum Γ states (Γ_c), followed by strong same-stage $\Gamma_c \to X$ scattering, ensures high *X*-valley population and subsequent high $X \to X$ leakage current at 300 K, even at low fields. Very good agreement with experiment is obtained at both cryogenic and room temperatures. © *2006 American Institute of Physics*. [DOI: 10.1063/1.2387485]

Room-temperature, pulsed mode operation of a 9 μm GaAs/AlGaAs intersubband quantum cascade laser (QCL) has been accomplished[1] by increasing the barrier-layer Al content from 33% to 45% within the conventional three-well active-region design. This important milestone in the midinfrared (mid-IR) GaAs/AlGaAs QCL technology was achieved due to the larger conduction band offset in the 45%-Al device than the 33% one.[2,3] With further increase of the barrier Al content, once the upper lasing level becomes aligned with the lowest *X*-valley state of the injection barrier, lasing is suppressed due to intervalley carrier transfer, which limits the emission wavelengths to above 8 μm.[4] Moreover, satellite-valley leakage can play a significant role in the carrier loss in InP-based mid-IR QCLs.[5] Therefore, it has become necessary to incorporate both Γ- and satellite-valley electronic transports into theoretical mid-IR QCL modeling. However, theoretical models[6–11] published so far have focused on the Γ-valley transport alone.

In this letter, we present a three-dimensional (3D) Monte Carlo simulation of two GaAs-based mid-IR QCLs with equivalent designs (the 33%-Al QCL of Refs. 2 and 3 and the 45%-Al QCL of Ref. 1) that takes both Γ- and *X*-valley transports into account. Designs of these two QCLs are equivalent,[1] since they have similar emitting wavelengths ($\sim$9 μm), threshold fields (48 kV/cm), dipole matrix elements (1.6 nm for the 33% QCL and 1.7 nm for the 45% QCL), and lifetimes in the upper lasing level (1.5 and 1.4 ps, respectively). Simulation reveals that the dominant *X*-valley leakage path in both lasers is $X \to X$ interstage scattering, exceeding the current due to direct interstage transfer between Γ and *X* valleys. The magnitude of the leakage current due to interstage $X \to X$ scattering depends on the occupation of the *X*-valley subbands, which are populated primarily by the same-stage scattering between the continuumlike Γ states (denoted as Γ_c for brevity) and the *X*-valley states. In the 33% QCL, localized Γ states (Γ_l for brevity) of the injector miniband couple strongly to the next-stage Γ_c states. Not only does this coupling lead to the well-recognized $\Gamma_l \to \Gamma_c$ leakage,[12,13] but, through populating Γ_c, also indirectly ensures high *X*-valley occupation and subsequent strong interstage $X \to X$ scattering. Consequently, at room temperature, the leakage current associated with the *X*-valley transport is very high in the 33% QCL even at fields significantly below threshold. In contrast, in the 45% structure, coupling of Γ_l states with the next-stage Γ_c states is weak due to better localization of the Γ_l states in the injector with higher barriers. Consequently, occupation of the *X*-valley states through same-stage $\Gamma_c \to X$ scattering is low, and the resulting leakage current due to interstage $X \to X$ scattering is also quite small up to high fields (above threshold). The calculated threshold currents for both the 33% QCL and 45% QCL are in very good agreement with the experimental data of Refs. 3 and 1, respectively, obtained for 2 mm long devices with low-loss, Al-free transverse waveguide design.[3]

Stationary electronic transport in mid-IR QCLs under typical operating conditions is incoherent[9] and can be described by a semiclassical Boltzmann-like equation.[8–10] We extend the Boltzmann-like equation to incorporate both Γ- and *X*-valley transports, namely,

$$\frac{d}{dt}f_{\mathbf{k}\alpha} = \sum_{\mathbf{k}'\alpha'} [P_{\mathbf{k}'\alpha'}^{\mathbf{k}\alpha} f_{\mathbf{k}'\alpha'}(1 - f_{\mathbf{k}\alpha}) - P_{\mathbf{k}\alpha}^{\mathbf{k}'\alpha'} f_{\mathbf{k}\alpha}(1 - f_{\mathbf{k}'\alpha'})], \tag{1}$$

where $|\mathbf{k}\alpha\rangle = |\mathbf{k}, \nu\ell\lambda\rangle$ denotes the 3D single-particle electronic state in the λth stage, ℓth valley (Γ and *X* valleys), νth subband, and with the in-plane wave vector $\mathbf{k}$. $f_{\mathbf{k}\alpha}$ is the distribution of electrons in the state $|\mathbf{k}\alpha\rangle$. $P_{\mathbf{k}'\alpha'}^{\mathbf{k}\alpha}$ is the total transition rate from $|\mathbf{k}'\alpha'\rangle$ to $|\mathbf{k}\alpha\rangle$. Translational symmetry of QCL structures enables us to simulate only charge transport over a central stage λ within the charge-conserving scheme[9] and limit interstage scattering to nearest neighbors ($\lambda' = \lambda \pm 1$).[6,8–10] Calculation of all the intrastage and nearest-neighbor interstage transition rates requires the knowledge of energy levels and wave functions in two full adjacent stages.

The Γ-valley states in two adjacent stages are obtained by solving the Schrödinger equation using the $\mathbf{k}\cdot\mathbf{p}$ method. The *X*-valley states are obtained by solving the effective mass equation, since the *X* valleys are well above the valence bands and the band mixing is negligible. The *X*-valley subbands form two distinctive sets according to the alignment of the principal axes of the effective mass tensor with the growth direction: (i) a set of nondegenerate states, corresponding to the *X* valley whose longitudinal axis is along the

[a)]Electronic mail: knezevic@engr.wisc.edu

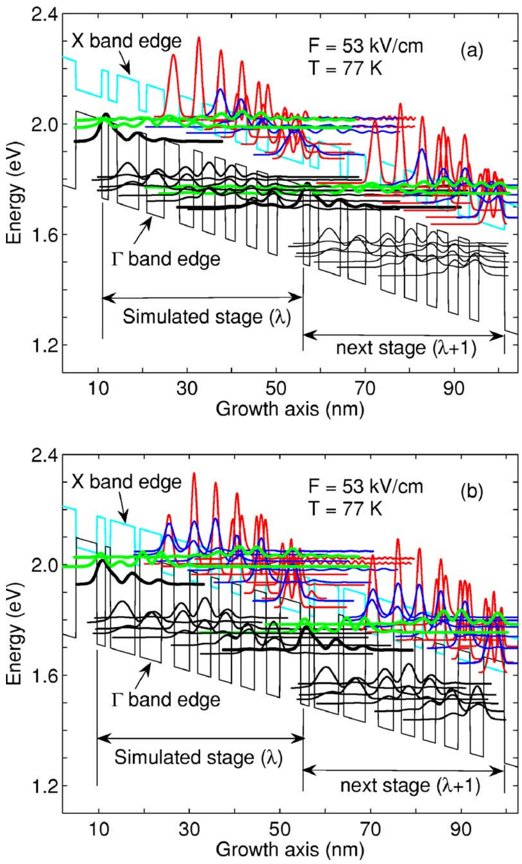

FIG. 1. (Color online) Energy levels and wave function moduli squared in two adjacent stages for the 33% QCL (a) and the 45% QCL (b). In each stage, the bold black line denotes the upper lasing level, while the thin black lines and two bold green lines represent the localized Γ_l states and continuumlike Γ_c states, respectively. $X1$ states (red lines) and $X2$ states (blue lines) in two adjacent stages are also shown.

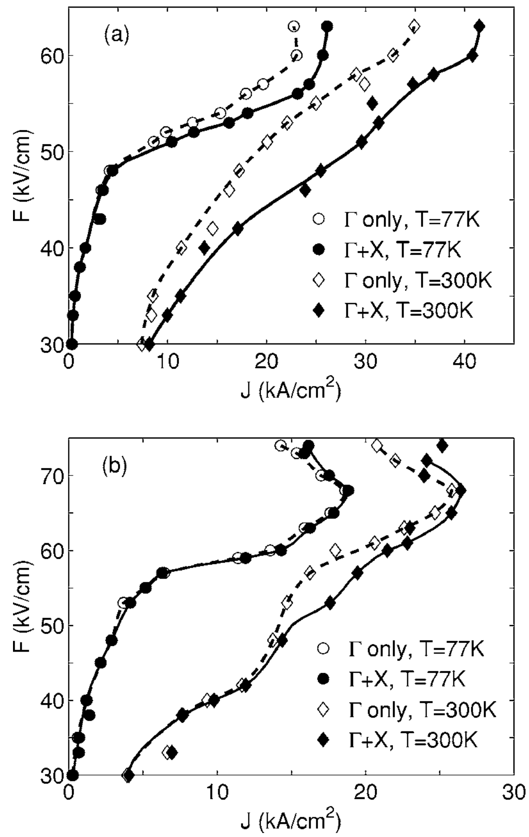

FIG. 2. Electric field vs current density characteristics for the 33% QCL (a) and the 45% QCL (b) at 77 and 300 K, with and without the X-valley transport included.

growth direction, denoted as $X1$ states (mixing of the $X1$ and Γ subbands is neglected[14]), and (ii) another set of doubly degenerate states, corresponding to the other two X valleys whose transverse axes are in the growth direction, denoted as $X2$ states.

Scattering mechanisms included are electron-LO-phonon and electron-electron (e-e) scattering among the Γ-valley subbands, X intravalley electron-LO scattering, and intervalley Γ-X and X-X scattering. Electron-phonon interaction is implemented assuming bulk phonons and quasi-two-dimensional electrons, while the e-e scattering is realized by employing the quasistatic multisubband screening model.[15–17] For all the scattering mechanisms, we include both the intrastage and interstage scattering events, with the latter yielding the current flow through the whole QCL device. The current density J is defined in terms of the carrier flux exiting the simulated λth stage across its left and right boundaries.[10]

Figure 1 illustrates the electronic structure of the 33% QCL [Fig. 1(a)] and the 45% QCL [Fig. 1(b)] at 77 K and above-threshold field of 53 kV/cm. The number of X states in each stage is the same and chosen such that the highest X subband is right above the second Γ continuumlike state and below other higher X levels. Since the X band edge is about 83 meV above the Γ band edge in the 33% QCL but ~30 meV below the Γ band edge in the 45% QCL, more X subbands are needed to properly simulate the latter device. In particular, at $F=53$ kV/cm and $T=77$ K, nine (ten) $X1$ subbands and four (six) $X2$ subbands are used in the 33% (45%) QCL simulation.

In Fig. 2, the applied field versus current density characteristics are shown for the 33% QCL [Fig. 2(a)] and the 45% QCL [Fig. 2(b)], with and without the X-valley transport included. At the temperature of 77 K, the calculated threshold current (J_{th}) for the 33% QCL with the X-valley transport included is 4.4 kA/cm^2 while the average experimental value is 5 kA/cm^2 (see Fig. 3 of Ref. 3). For the 45% QCL, the calculated J_{th} is 2.9 kA/cm^2 while the experimental value obtained in Ref. 1 equals 4 kA/cm^2. Both threshold currents agree with the experimental data very well, especially considering that the simulation does not account for the losses at the lateral waveguide (ridge) edges. Subsequent experimental work[18] on 45% QCLs, where the ridge edges had smooth surfaces, due to wet chemical etching, and no absorbing material, reported $J_{\mathrm{th}}=3$ kA/cm^2, in excellent agreement with our calculation. The 33% QCL shows higher J_{th} in both theory and experiment than the 45% QCL. At the low temperature of 77 K, this difference (about 1 kA/cm^2 at threshold) is primarily due to strong $\Gamma_l \rightarrow \Gamma_c$ interstage leakage, stemming from poor localization of the Γ_l states in the 33% QCL and their large overlap with the next-stage Γ_c states [Fig. 1(a)]. X-valley transport in the 33% QCL amounts for a small additional leakage current (0.4 kA/cm^2 at threshold). In the 45% QCL, the injector states are well localized and thus the leakage current due to both $\Gamma_l \rightarrow \Gamma_c$ interstage scattering and X-valley transport is negligible up to very high fields.

At room temperature, the simulated threshold current for the 33% structure with the X-valley transport included is

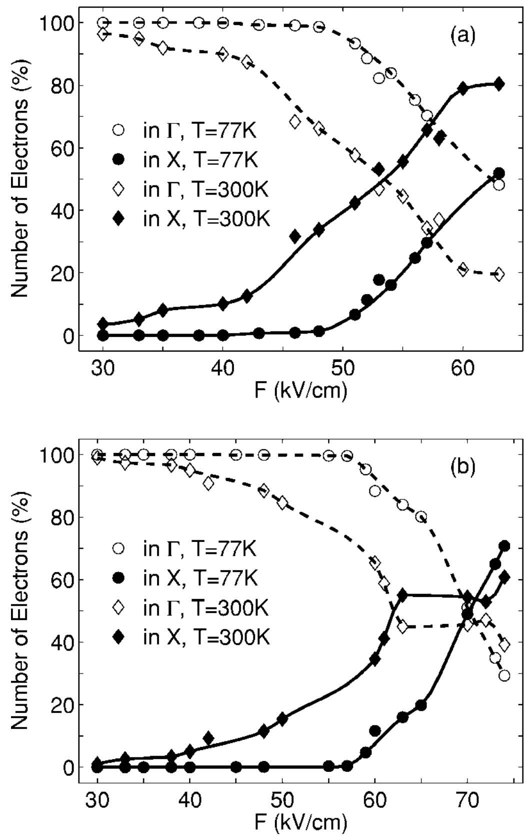

FIG. 3. Percentage of electrons in Γ and *X* valleys vs applied field for the 33% QCL (a) and the 45% QCL (b) at 77 and 300 K.

very high (J_{th}=25.5 kA/cm^2), which can help explain why the 33% QCL could not lase at 300 K. For the 45% QCL, the calculated J_{th}=14.4 kA/cm^2 with the *X* valley included is in very good agreement with $J_{th} \approx 16.7$ kA/cm^2 obtained in experiment,[1] especially considering that, as before, the simulation does not account for ridge edge losses. As seen by comparing Figs. 2 and 3, at 300 K, the increase in the *X*-valley leakage current in both lasers follows the increase in the *X*-valley population (also true at 77 K, although somewhat less obvious). This is due to the fact that $X \rightarrow X$ interstage scattering is the dominant leakage mechanism, more efficient than direct interstage scattering between Γ and *X*. What is striking is how large the *X*-valley leakage current is in the 33% QCL even at fields significantly below threshold (at threshold, the *X*-valley leakage current is about 8 kA/cm^2). What happens is that *X*-valley states are populated predominantly by efficient same-stage scattering from Γ_c. This intrastage scattering does not contribute to the current directly and is very efficient at room temperature in both QCLs, as seen by the large wave function overlap in both Figs. 1(a) and 1(b). The inverse scattering (i.e., intrastage from *X* to Γ_c) is weaker because of the lighter mass in Γ_c. In the 33% QCL, owing to strong interstage carrier scattering from Γ_l to Γ_c, followed by intrastage $\Gamma_c \rightarrow X$, the *X*-valley is filled efficiently, and consequently interstage $X \rightarrow X$ scattering produces a high leakage current. In the 45% QCL, in contrast, Γ_c does not get filled through $\Gamma_l \rightarrow \Gamma_c$ scattering because their overlap is small [Fig. 1(b)], which explains the negligible below-threshold *X*-valley leakage current [Fig. 2(b)]. However, at very high fields, Γ_c gets filled by intrastage scattering (i.e., high fields lead to high electronic temperatures), which then enhances the leakage current due to interstage $X \rightarrow X$ scattering. The mechanisms of *X*-valley leakage described above hold at 77 K as well, but leakage is much less pronounced because of few active phonons that enable intervalley scattering.

In summary, we have presented a Monte Carlo simulation incorporating the effects of *X*-valley transport on the operation of equivalent-design GaAs/$Al_{0.33}Ga_{0.67}As$ and GaAs/$Al_{0.45}Ga_{0.55}As$ QCLs. The 33% QCL has a higher *X*-valley leakage current than the 45% QCL at both 77 and 300 K. The reason is strong coupling between the injector states and the next-stage continuumlike states in the 33% QCL, which facilitates filling of the *X*-valley states through efficient intrastage $\Gamma_c \rightarrow X$ scattering. With high *X*-valley occupation, interstage $X \rightarrow X$ scattering yields a high leakage current, even at low fields, in the 33% QCL at 300 K. In contrast, good localization of the injector miniband states in the 45% QCL ultimately leads to low *X*-valley leakage current up to high fields. The simulated J_{th} with the *X*-valley leakage included is in very good agreement with experiment for both QCLs at 77 and 300 K.

The authors gratefully acknowledge valuable discussions with C. Sirtori and support from the Wisconsin Alumni Research Foundation (WARF).

[1] H. Page, C. Becker, A. Robertson, G. Glastre, V. Ortiz, and C. Sirtori, Appl. Phys. Lett. **78**, 3529 (2001).
[2] C. Sirtori, P. Kruck, S. Barbieri, P. Collot, J. Nagle, M. Beck, J. Faist, and U. Oesterle, Appl. Phys. Lett. **73**, 3486 (1998).
[3] C. Sirtori, P. Kruck, S. Barbieri, H. Page, J. Nagle, M. Beck, J. Faist, and U. Oesterle, Appl. Phys. Lett. **75**, 3911 (1999).
[4] L. R. Wilson, D. A. Carde, J. W. Cockburn, R. P. Green, D. G. Revin, M. J. Steer, M. Hopkinson, G. Hill, and R. Airey, Appl. Phys. Lett. **81**, 1378 (2002).
[5] W. T. Masselink, M. P. Semtsiv, S. Dressler, M. Ziegler, N. Georgiev, T. Dekorsy, and M. Helm, Proc. SPIE **5738**, 13 (2005).
[6] D. Indjin, P. Harrison, R. W. Kelsall, and Z. Ikonic, J. Appl. Phys. **91**, 9019 (2002).
[7] H. Callebaut and Q. Hu, J. Appl. Phys. **98**, 104505 (2005).
[8] O. Bonno, J.-L. Thobel, and F. Dessenne, J. Appl. Phys. **97**, 043702 (2005).
[9] R. C. Iotti and F. Rossi, Phys. Rev. Lett. **87**, 146603 (2001).
[10] R. C. Iotti and F. Rossi, Rep. Prog. Phys. **68**, 2533 (2005).
[11] S.-C. Lee and A. Wacker, Phys. Rev. B **66**, 245314 (2002).
[12] S. Barbieri, C. Sirtori, H. Page, M. Stellmacher, and J. Nagle, Appl. Phys. Lett. **78**, 282 (2001).
[13] D. Indjin, P. Harrison, R. W. Kelsall, and Z. Ikonic, Appl. Phys. Lett. **81**, 400 (2002).
[14] O. E. Raichev, Phys. Rev. B **49**, 5448 (1994).
[15] S. M. Goodnick and P. Lugli, Phys. Rev. B **37**, 2578 (1988).
[16] S. M. Goodnick and P. Lugli, Appl. Phys. Lett. **51**, 584 (1987).
[17] M. Moško, A. Mošková, and V. Cambel, Phys. Rev. B **51**, 16860 (1995).
[18] C. Sirtori, H. Page, C. Becker, and V. Ortiz, IEEE J. Quantum Electron. **38**, 547 (2002).